ELSEVIER

Journal of Structural Geology 28 (2006) 2156–2168

JOURNAL OF STRUCTURAL GEOLOGY

www.elsevier.com/locate/jsg

Kinematic analysis of radial structures around Irnini Mons, Venus

Debra L. Buczkowski*

Johns Hopkins University, Applied Physics Laboratory, Laurel, MD 20723, USA

Received 18 August 2004; received in revised form 20 February 2006; accepted 5 April 2006
Available online 19 June 2006

Abstract

Radial structures to the north-east of Irnini Mons are discernable as ridges at the full Magellan image resolution of 75 m/pixel using FMAP tiles. While a magma source modeled as a pressurized hole in an elastic plate usually allows for only extensional radial structures, the perturbation of regional stresses around the hole can explain the presence of radial ridges. Sixteen numerical models were run to see what effect changes in magma pressure and regional stresses had on the magnitude of the maximum principal stresses and the orientation of potential features around a hole in a plate. These models were arranged into four groups based on model input and setup: 1) uniaxial compressive stress; 2) uniaxial tensile stress; 3) biaxial stress; and 4) multiple holes. Nine of the sixteen models result in radial ridges in the orientation observed around Irnini Mons; all of these models incorporate a regional N-S compression. Flows from Irnini Mons are superimposed on an older, regional plains material deformed by a regional set of east-west trending wrinkle ridges, implying a regional north-south compression affected the area. The existence of radial ridges on the Irnini flows implies that the regional N-S compression that caused the E-W trending wrinkle ridges was still active during the formation of Irnini Mons. However, the magnitude of the regional compressive stress required for radial ridge formation could be 1–5 MPa less than the compressive strength of the material, indicating that radial ridges could form after wrinkle ridge formation has ceased.

Keywords: Venus; Irnini Mons; Kinematic analysis; Numerical modeling

1. Introduction

Although relatively simple structurally, the regional plains of Venus are the planet's dominant terrain, covering ~75% of the surface. Impact craters on the regional plains are randomly distributed and show few signs of degradation (Phillips et al., 1991; Schaber et al., 1992; Strom et al., 1994; Turcotte et al., 1998), implying that the emplacement of the plains occurred during a rapid resurfacing event. The crater abundance on the plains indicates that the average age of most of the surface of Venus is a few hundred million years, although a quantitative average age is debated (300–500 Ma, Schaber et al., 1992; 400–800 Ma, Phillips et al., 1992; 190–599 Ma, Strom et al., 1994; 400–1600 Ma, Zahnle and McKinnon, 1996; 700–800 Ma, McKinnon et al., 1997). There is also some debate on the emplacement time span (Phillips et al., 1992; Strom et al., 1994; Price, 1997; Hauck et al., 1998; Collins et al., 1999; Basilevsky et al., 1999; Campbell, 1999; Basilevsky and Head, 2000). Such a resurfacing would have had to have been nearly global in scale, considering the areal extent of the regional plains.

The regional plains also are consistently deformed by minor structures. Wrinkle ridges, fabrics of linear structures, and small graben are pervasive, implying a widespread pattern of shallow crustal stress (McGill, 1993; Sandwell et al., 1997; Bilotti and Suppe, 1999; Solomon et al., 1999; Basilevsky and Head, 2000) that post-dates the rapid resurfacing. The stress states both during and after the resurfacing event are described in many different tectonic models (e.g., Banerdt, 1986; Phillips and Hansen, 1994; Hansen et al., 1997; Basilevsky and Head, 1998; Solomon et al., 1999). Many of these models support either a directional tectonic

* Formerly at: Geosciences Department, University of Massachusetts, Amherst, MA 01003, USA.
E-mail address: debra.buczkowski@jhuapl.edu

0191-8141/$ - see front matter © 2006 Elsevier Ltd. All rights reserved.
doi:10.1016/j.jsg.2006.04.005

history (Basilevsky et al., 1997; Basilevsky and Head, 1998), in which particular geological processes are restricted to particular time periods, or a non-directional tectonic history (Guest and Stofan, 1999), in which geological processes can occur repeatedly throughout history. The predictions made in these models can be tested with a detailed structural analysis. If the distribution, orientation and relative timing of these structures agree with a model or models, much can be determined about the internal dynamics of Venus for the last few hundred million years.

Geologic mapping is a fundamental part of any attempt to understand the crustal history of a planet. The V-20 quadrangle (McGill, 2000) is roughly centered on Irnini Mons, and the area immediately around this volcano is complex and interesting (Fig. 1). The work presented here is an analysis of structures radial to Irnini Mons, found to the northeast and discernable as ridges at the full Magellan image resolution of 75 m/pixel using FMAP tiles (Fig. 2). By determining the relative ages of the structures and units, a history of the orientations of the principal stresses during the formation of the local regional plains, as well as Eistla Regio, can be derived. Determining the specific sequence of stress orientations for regions on Venus is the first step in constraining the various existing tectonic models, since most of these models predict some specific sequence of stress orientations.

Section 2 will summarize the mapped structural features and geologic units immediately around Irnini Mons, and includes a brief description of radar interpretation and implications for the radial features around the volcano. Section 3 introduces the analytical model of a hole in a plate, with a brief background of its use in previous studies, and summarizes five possible explanations for the presence of ridges radial to Irnini Mons. Section 4 presents the setup and results of a new parametric study of regional stresses on a pressurized hole. In Section 5 the model results are compared to the observations around Irnini Mons and a possible sequence of stress states that could have resulted in ridges forming radial to the volcano as primary features is discussed. Finally, in Section 6 a possible timeline of events is presented.

2. Observations

2.1. Structural features

Irnini Mons is a volcano centered at 14 °N, 16 °E in the V-20 quadrangle of Venus. The Irnini Mons volcanic edifice is about 475 km wide and 1.75 km high (McGill, 2000). The volcano is capped by Sappho Patera, a 225 km diameter depression rimmed by both concentric graben and a large circumferential ridge (Fig. 1b). Sappho Patera has been characterized by Stofan et al. (1992) as a corona or corona-like feature; simply, a corona is a circular to elongate feature surrounded by multiple concentric ridges thought to be formed by hot spots.

The structural features surrounding Irnini Mons are illustrated in Fig. 1b. The volcano is crossed by two rift systems, the north-south trending Badb Linea and an older rift which incorporates Guor Linea to the northwest and Virtus Linea to the southeast. Large surrounding structural complexities include four coronae and Anala Mons, a 550 km diameter, 2.25 km high volcano almost directly to the south of Irnini. Small-scale structures include two sets of wrinkle ridges, low sinuous ridges common on the Moon, Mars and Venus. There are also two overlapping sets of radar-bright lineations that can not be resolved as either graben or ridges (Fig. 1a).

2.2. Geology

As is shown in Fig. 1a, McGill (2000) mapped flows and other deposits from Irnini Mons that are superimposed on an older, regional plains material. These superposed materials include: 1) a shield plains unit (fs) younger than the regional plains (prb); 2) flows from Irnini Mons (fl and fhl) that are also younger than the plains (prb); and 3) a smooth plains unit (ps) that is younger than the flows (fl and fhl). The regional plains material (prb) has abundant wrinkle ridges in at least two sets: one trending generally east-west and another concentric to Irnini Mons.

The shield plains unit (fs) is abundantly covered with small domes. Although the shield plains are crossed by wrinkle ridges, they are not necessarily oriented in the same manner as the wrinkle ridges on the background regional plains (prb). Graben associated with Badb Linea cut through the shield material, which overlies a lineated plains material (pl), interpreted as being a relatively old plain of deformed volcanic rocks (McGill, 2000).

The Irnini flows are described by McGill (2000) as two units. The first is interpreted as basaltic lava flows (fl), while the second is basaltic lava overlain by a thin pyroclastic veneer (fhl). Both units are free of wrinkle ridges, but do show fabrics of lineations and graben. They seem to overlie every unit save the smooth plains (ps). Radial features on top of the Irnini flows (fl and fhl) were mapped by McGill (2000) as lineations or graben, as resolution allowed.

The smooth plains unit (ps) is superposed on the Irnini flows and most of the structures (McGill, 2000). There are no wrinkle ridges, but small domes and some lineations are visible, though apparently covered.

2.3. Radar backscatter of linear features radial to Irnini Mons

As with solar illumination, radar illumination of a planetary structure highlights the surface that faces the source (Campbell, 2002). If a topographic low, such as a graben, were being imaged, the surface away from the radar look direction would be the surface facing the radar system and would be illuminated (Fig. 3). The graben surface closer to the look direction would be facing away from the radar system and would appear relatively dark. Thus a linear feature in a radar image that is composed of a dark band then a bright band is some type of linear topographic low, such as a graben, trough or fracture (Fig. 4). A topographic

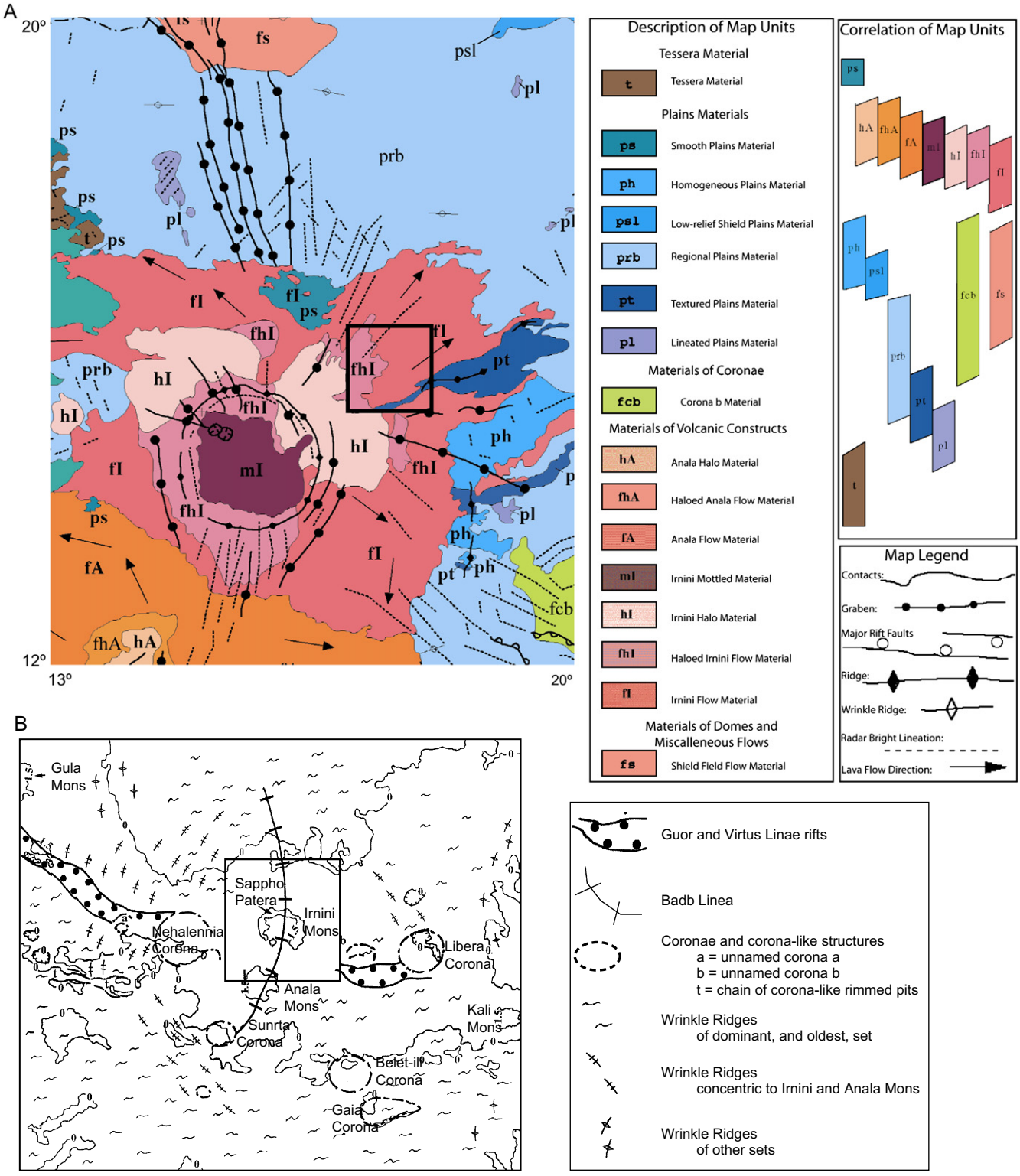

Fig. 1. a) Geologic map of Venus from 12–20°N, 13–20°E, adapted from the Sappho Patera Quadrangle (V-20) as mapped by McGill (2000). Inset box (roughly 100 km on each side) marks location of Fig. 2. b) Tectonic elements of V-20, as mapped by McGill (2000). Inset box shows region mapped in Fig. 1a.

high, such as a ridge, would have the opposite appearance (Fig. 3). The surface closer to the look direction would be facing the radar source and would be illuminated, while the further surface would be facing away and thus dark (Fig. 5). Commonly, resolution does not allow the discernment of both a bright and dark part of a linear feature. Where only a bright line is visible the feature is referred to as a lineation, to avoid misidentification.

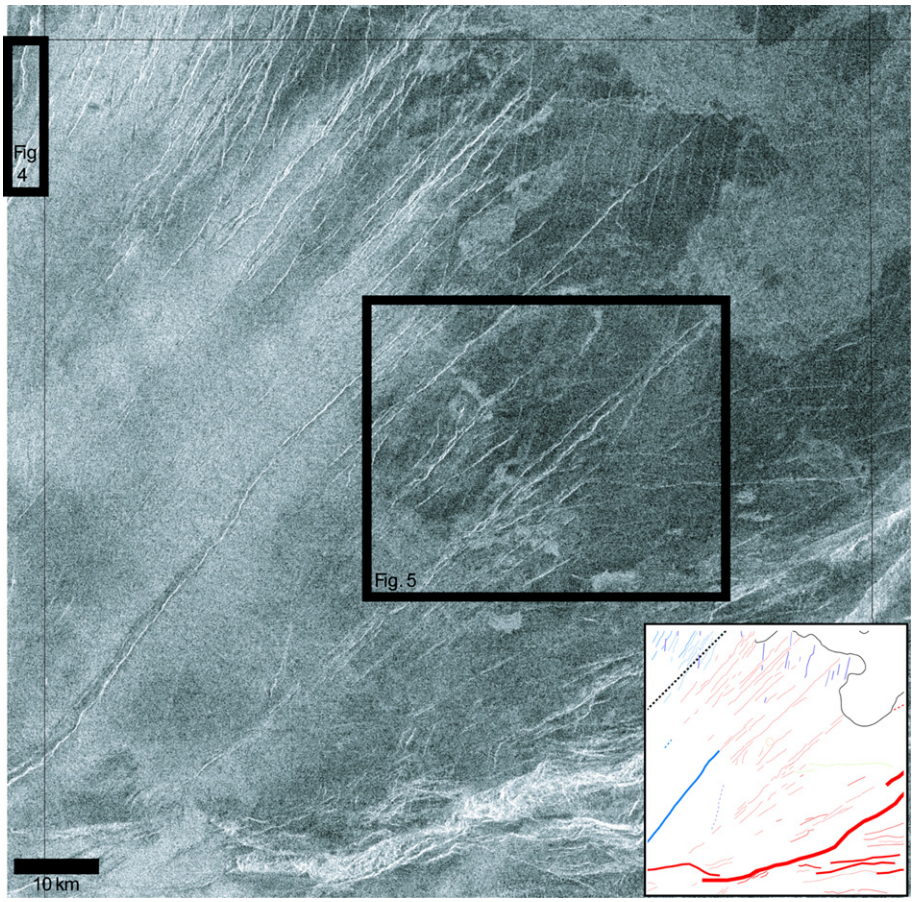

Fig. 2. High resolution (75 m/pixel) SAR image of 15°–16°N, 17°–18°E, located in inset box of Fig. 1. Black rectangles indicate locations of Figs. 4 and 5. Inset box shows tectonic of same region. Red are radial ridges; dark blue are radial graben; purple are N-S trending lineations; light green are regional, E-W wrinkle ridges; black outlines a specific flow. Width of line indicates relative size of feature. Black dotted line indicates an orientation of N45E from the center of Irnini Mons.

The most interesting of the lineation fabrics appears to the north of Irnini Mons, on the regional plains between the northern shield flows (fs) and the Irnini flows (fI and fhI). A northwest-trending set of lineations overlaps a northeast-trending lineation set in the area. Lineations vary in length from 1–2 km (the limit of detection) to many hundreds of kilometers (McGill, 2000). Further complicating the immediate region are graben associated with Badb Linea and closely spaced, E-W trending wrinkle ridges. Small domes are also present.

From approximately N45E to N75E relative to Irnini (Fig. 2) the difference in radar backscatter in high resolution images (75 m/pixel) indicates that the radial features are topographic highs (Fig. 5), although they are too narrow to be resolved in altimetry data sets. These features are similar to the "horst-like lineaments" identified by Ernst et al. (2003). Unlike the textured plains material (pt) unit of arcuate ridges mapped by McGill (2000), which is directly south, these ridges are on top of the Irini flows and cannot be an older feature. To the north the radial features appear to be graben, also located on top of the Irnini flows (Fig. 4). Due north, the radial graben become indistinguishable from the graben associated with the Badb Linea rift.

3. Structures radial to Irnini Mons

3.1. Models for the formation of radial features on Venus

Grosfils and Head (1994) identified 163 radial lineament systems in the Magellan radar data, where the lineaments were graben, fissures and fractures. These radiating systems, sometimes known as radially fractured centers or RFCs (Grindrod et al., 2005), are oriented around a variety of central features, including volcanoes (Head et al., 1992) and coronae (Stofan et al., 1992). Over half of the RFCs are associated with topographically high domes (Grosfils and Head, 1994).

There are two schools of thought on how RFCs form. One interpretation is that the radial graben and fractures are the surface expression of the propagation of shallow dikes (e.g. McKenzie et al., 1992; Parfitt and Head, 1993; Grosfils and Head, 1994; Koenig and Pollard, 1998). The second group of models invokes domical uplift due to the rising of mantle diapirs (e.g. Stofan et al., 1992; Cyr and Melosh, 1993). It is likely that both processes play some part in the formation of the radial structures, as does lithospheric loading (McGovern and Solomon, 1998). However, fractures due solely to uplift are not as common as those due to dike emplacement (Grosfils

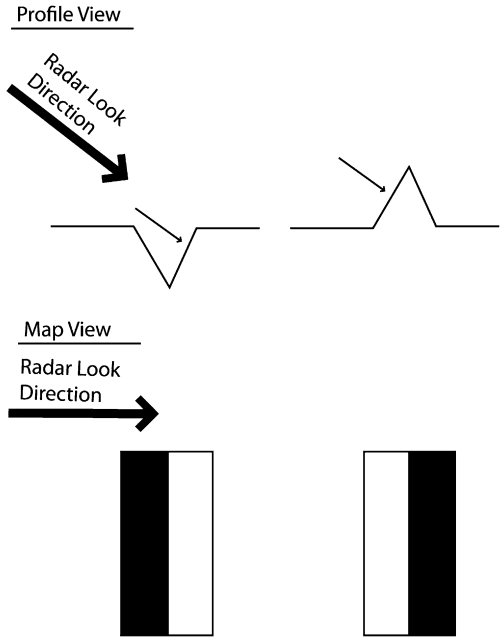

Fig. 3. A cartoon illustrating how graben and ridges would appear in a radar image. If a topographic low such as a graben were being imaged by a radar system, the surface further from the look direction would be facing the radar system and would appear brighter than the opposite face. If a topographic high such as a ridge were being imaged, the surface closer to the look direction would be illuminated.

and Head, 1994) and the strain at the large radial graben is primarily due to dikes as opposed to uplift (Grindrod et al., 2005).

3.2. The hole- in-a-plate model

The hole-in-a-plate model is a well established method of explaining the radial dikes and corresponding graben present around volcanic bodies on both Earth (e.g. Ode, 1957; Jaeger and Cook, 1979) and Venus (e.g. McKenzie et al., 1992; Koenig and Pollard, 1998). An empty hole in an elastic plate perturbs a regional stress field close to the hole, although not at infinity. For volcanoes, the change in material properties from the surrounding rock to a magma-filled chamber allows us to consider the chamber as "soft" and thus effectively empty. Although they drastically simplify the geology of a volcano and its magma source, the two-dimensional hole-in-a-plate model and its three-dimensional counterpart (a spherical cavity in an elastic half space) have been shown to describe the deformation at volcanoes and other magmatic bodies quite well (e.g. Ode, 1957; McKenzie et al., 1992; Koenig and Pollard, 1998; Sturkell et al., 2003; Grindrod et al., 2005).

Equations (compression positive) have been derived (Jaeger and Cook, 1979) to describe the radial stresses σ_{RR}, circumferential stresses $\sigma_{\theta\theta}$ and shear stresses $\tau_{R\theta}$ that result around the pressurized hole, where P is magma pressure, R is the magma source radius, r is the distance from the center of the hole, and σ_{11} and σ_{22} are the regional stresses. θ is the orientation around the hole, relative to its center, where 0° and 180° are aligned with the σ_{11} direction; 90° and 270° are parallel to the σ_{22} direction.

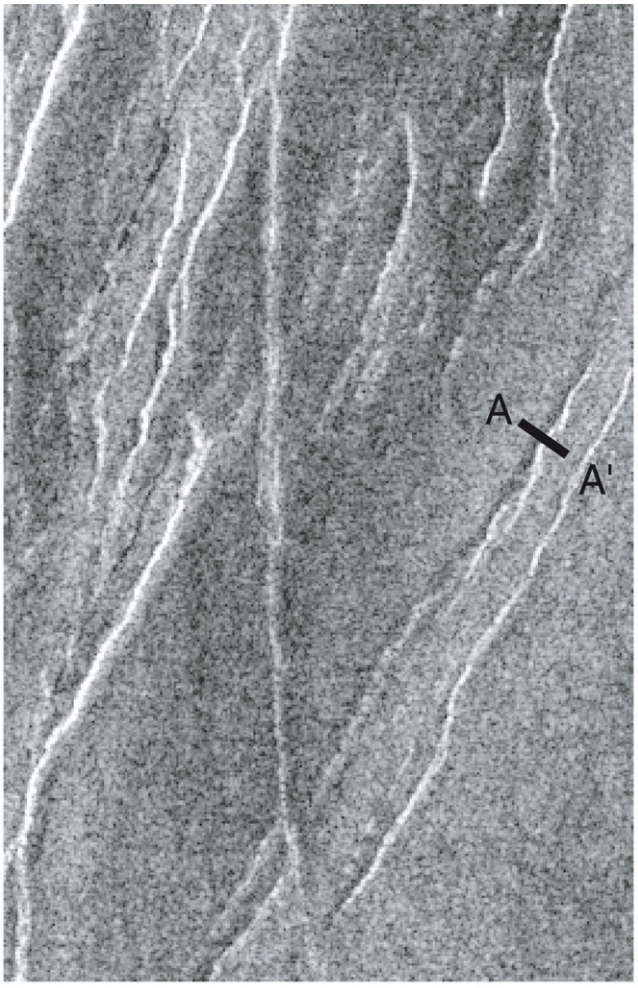

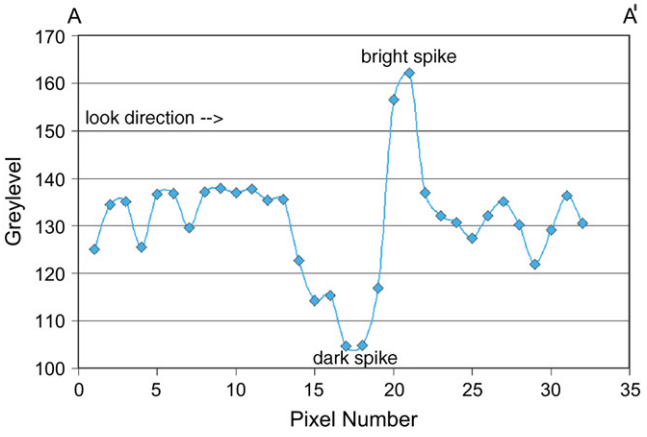

Fig. 4. Enlargement of radial linear features in inset box of Fig. 2. Radar backscatter pattern indicates that these features are graben. Profile A to A′ shows a darkness spike followed by a brightness spike, indicative of a topographic low.

$$\sigma_{RR} = P\left(\frac{R}{r}\right)^2 + \frac{1}{2}(\sigma_{11}+\sigma_{22})\left(1-\left(\frac{R}{r}\right)^2\right) + \frac{1}{2}(\sigma_{11}-\sigma_{22})\left(1-4\left(\frac{R}{r}\right)^2+3\left(\frac{R}{r}\right)^2\right)\cos 2\theta \qquad (1)$$

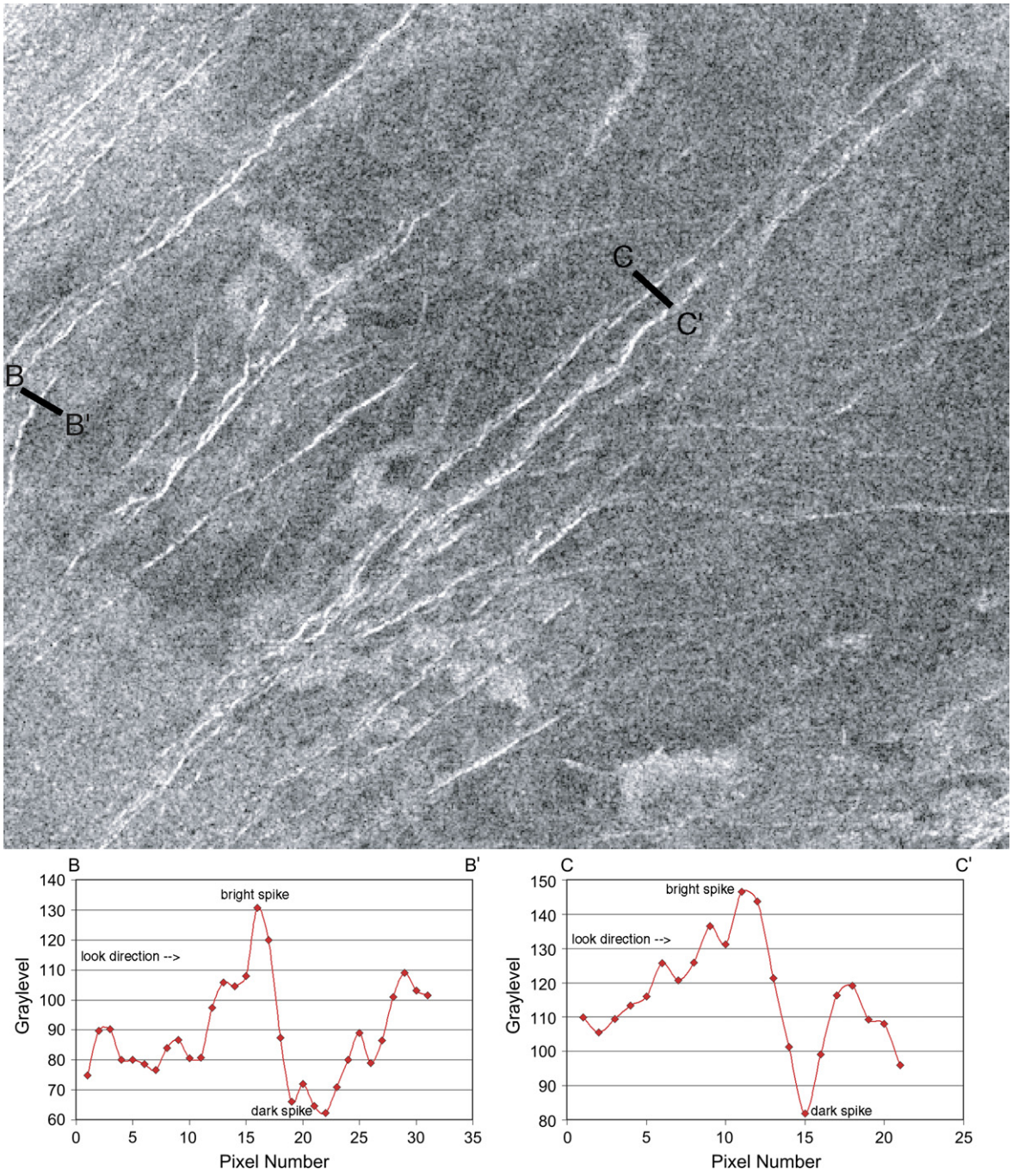

Fig. 5. Enlargement of radial linear features in inset box of Fig. 2. Radar backscatter pattern indicates that these features are ridges. Profiles B to B′ and C to C′ show a brightness spike followed by a darkness spike, indicative of a topographic high.

$$\sigma_{\theta\theta} = -P\left(\frac{R}{r}\right)^2 + \frac{1}{2}(\sigma_{11}+\sigma_{22})\left(1+\left(\frac{R}{r}\right)^2\right) - \frac{1}{2}(\sigma_{11}-\sigma_{22})\left(1+3\left(\frac{R}{r}\right)^2\right)\cos 2\theta \quad (2)$$

$$\tau_{R\theta} = \frac{1}{2}(\sigma_{11}-\sigma_{22})\left(1+2\left(\frac{R}{r}\right)^2-3\left(\frac{R}{r}\right)^4\right)\sin 2\theta \quad (3)$$

Structures will only form where the maximum principal stresses are greater than the strength of the material. The tensile strength of Venus rocks is fairly well constrained to −0.2 to −2 MPa (Schultz, 1993), but the compressive strength ranges anywhere between <10 to 50 MPa (Schultz, 1993). If regional stresses are negligible, these equations yield results consistent with radial graben everywhere around the hole (Fig. 6). The radial compressive stress produced does not exceed the compressive strength of the material, and no circumferential ridges form.

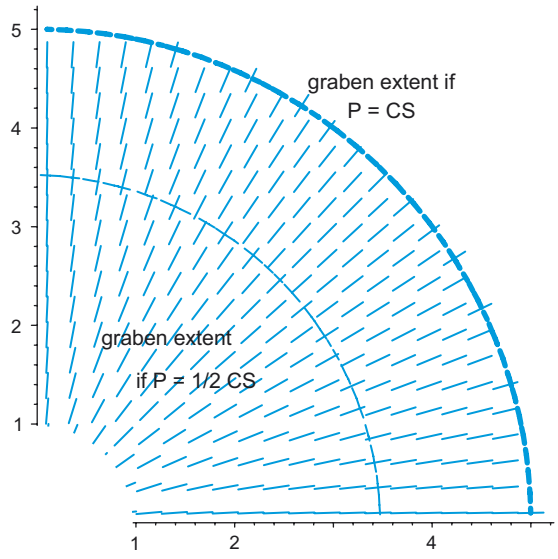

Fig. 6. Results of modeling a magma source as a hole in a plate. Figure shows orientation and extent of features formed around a magma source exerting pressure in the absence of a regional stress field ($\sigma_{11} = \sigma_{22} = 0$). Graben form radial to the magma source but no ridges form. Figure shows only the north-east quadrant; pattern is symmetric around the magma source. Axes are distance from the center of the magma source in units of magma source radius.

3.3. Explaining radial ridges

The hole-in-a-plate model can thus explain the presence of graben radial to a volcano. However, the features radial to Irnini Mons from N45E to N75E are linear topographic highs. Some possible explanations are that the features are: 1) exposed radial dikes; 2) tilted half-graben blocks; 3) horsts bordering flooded graben; 4) tectonically inverted graben; or 5) true ridges formed by compression. These five possible explanations are explored.

3.3.1. Exposed radial dikes

Shallow dike emplacement is a persistent theory for the formation of radial systems of graben, fissures and fractures on Earth (Ode, 1957; Muller and Pollard, 1977; Ernst et al., 1995, 2001) and Venus (e.g. McKenzie et al., 1992; Parfitt and Head, 1993; Grosfils and Head, 1994; Koenig and Pollard, 1998). As discussed in the previous section, magma pressure causes circumferential tensile stresses, which can result in radiating dikes. Localized stresses above the subsurface dikes can result in the creation of surface fissures that are as wide as the depth to the top of the dike (Pollard and Holzhausen, 1979). On Earth, erosion can expose these radial dikes as freestanding topographic highs, such as those around the Spanish Peaks of Colorado (Ode, 1957; Muller and Pollard, 1977). If subsurface dikes around Irnini Mons had been exhumed they might have the backscatter signature observed in Fig. 2. However, on Venus there is very little erosion (Arvidson et al., 1992), leaving no known mechanism for their exposure.

3.3.2. Tilted fault blocks (half-graben)

Half-graben form when the hanging wall block of a normal fault tilts over toward the fault due to rotation during displacement (“reverse drag”). As the original fault block tilts other fault blocks break off, forming a series of half-graben (Fig. 7a). The peaks of tilted fault blocks are topographic highs that are the “ranges” of the Basin and Range Province of the United States. On Venus, similar fault block tips could resemble those topographic highs in Fig. 2. However, if the features around Irnini Mons are half-graben, there should be an overreaching graben signature around the tilted fault blocks to represent the original normal fault (Fig. 7a). Such a signature is not visible.

3.3.3. Horsts bounding flooded graben

Graben bounded by two adjacent normal faults have corresponding topographic highs called horsts (Fig. 7b). The topographic highs in Fig. 2 could conceivably be sorted in pairs, which could then be interpreted as the matched horsts surrounding a graben. However, as is seen in Fig. 7b, a freestanding horst is bound on both sides by graben; there can be graben without bounding horsts, but not horsts without flanking graben. The radial lineations from N45E to N70E are consistently topographic highs (Fig. 2). There is no backscatter signature indicating a graben-horst-graben pattern of structures.

3.3.4. Tectonically inverted graben

DeShon et al. (2000) observed ridges in Rusalka Planitia that were aligned in the same direction as a fracture set that cut an older flow. Their interpretation was that a younger flow filled part of the fracture set. After this younger flow had solidified a strike-oblique contraction caused the fill to invert, creating ridges. This model is a plausible explanation for the existence of the radial topographic highs observed

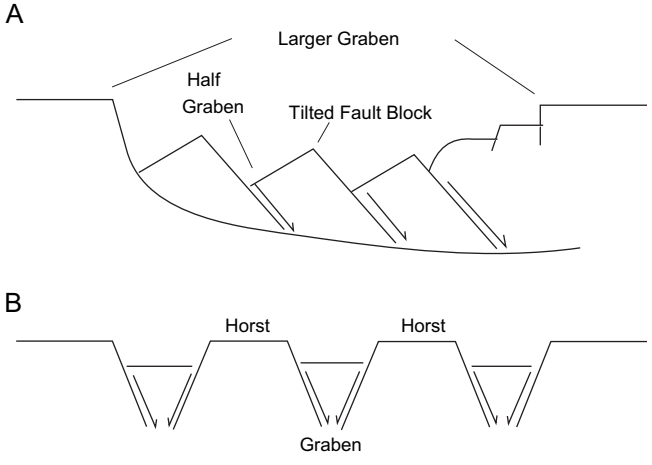

Fig. 7. a) Sketch of tilted fault blocks that were once part of the hanging wall of a normal fault. Note that half-graben is bound by a fault on only one side. The radar return would show prominent dark band (low) on the slope nearest the radar, which would match a graben return signature, not a ridge signature. b) Sketch of horsts. Graben are bound by two normal faults. The radar return would indicate a set of parallel graben, not ridges.

around Irnini Mons, and will be considered further in the discussion (Section 5).

3.3.5. Compressional ridges

Magma pressure alone can explain radial graben, but can not explain the presence of radial ridges. However, the east-west (±20°) trending wrinkle ridges dominating the regional plains of the V-20 quadrangle imply that at one time a regional north-south compression affected the Irnini Mons area. If this compression was ongoing while Irnini Mons was active, the regional stress field would be perturbed around the Irnini magma source. The perturbation of a north-south regional compressive stress σ_{11} around a pressurized hole is such that at angles 0° (north) and 180° (south) the maximum principal stresses close to the hole are tensile, while at angles 90° (east) and 270° (west) the maximum principal stresses close to the hole are compressive (Figs. 8–11). The angle θ at which maximum principal stresses change from tension to compression depends upon the distance from the hole and the relative magnitudes of magma pressure and the regional compression. While in the simple model resultant stresses would be symmetric around the hole, structural complexities to the south and west of Irnini Mons (Fig. 1b) restrict the predicted pattern of radial ridges as well as graben to the region northeast of the volcano. Incorporating these complexities into the model can increase our understanding of the sequence of events that resulted in the observed features.

4. Parametric study of regional stresses on a pressurized hole

Previous hole-in-a-plate models (e.g. Ode, 1957; McKenzie et al., 1992; Koenig and Pollard, 1998) were all specifically attempting to explain the orientation of tensile features radial to a magma source. The observation of topographic highs radial to Irnini Mons requires a model that predicts compression circumferential to the volcano, thus yielding radial ridges. A first-order model, consistent with the successful models mentioned above, was designed to perform this test.

Other studies of Earth and Venus have explored in more detail the formation and propagation of dikes from shallow magma chambers (e.g. Parfitt and Head, 1993; Grosfils and Head, 1997; Gudmundsson, 1984, 1986, 1988). On Venus, shallow magma reservoirs are predicted at intermediate elevations while deep reservoirs with conduits are predicted at highest elevations (Head and Wilson, 1992). It is debatable which conceptual model is the best representation of the magma source under Irnini Mons. However, in a two dimensional model the cross-section of either a shallow spherical magma chamber or the upper portion of a magma conduit can be represented as a circular hole in a plate (Koenig and Pollard, 1998). While some models indicate that magma reservoirs on Venus are ellipsoidal rather than spherical (e.g. Head and Wilson, 1992; Grosfils and Head, 1997), simplifying the magma source to a spherical shape with a circular cross-section is not inappropriate for a first-order model (e.g. Grindrod et al., 2005).

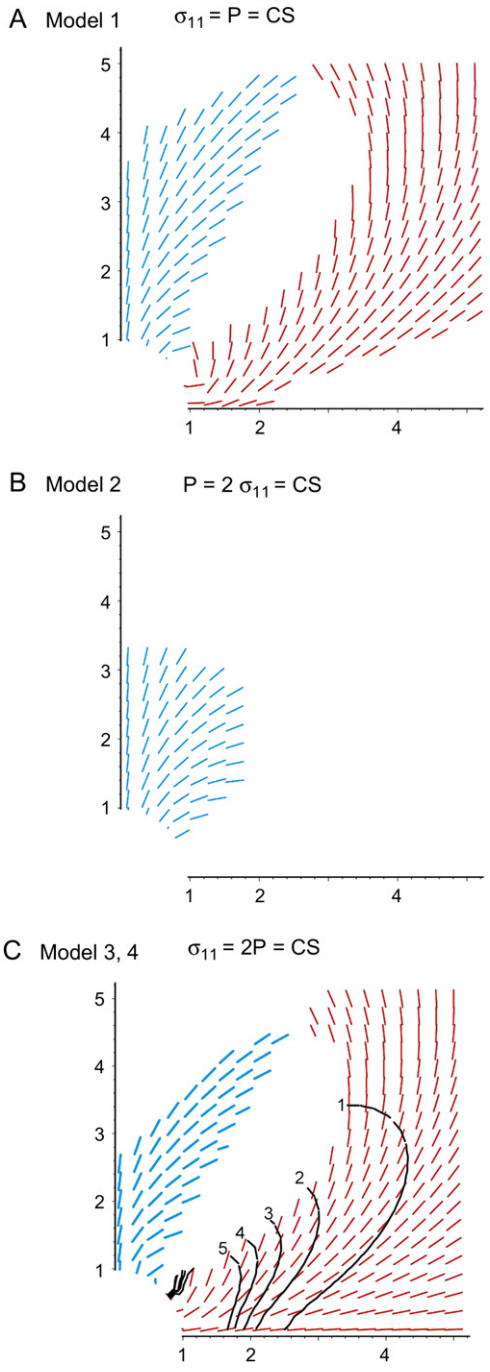

Fig. 8. Orientation and extent of structures in the presence of a uniaxial N-S compressive stress field. Blue are graben, red are ridges. Axes are distance from the center of the magma source in units of magma source radius. Parameters vary as noted. Contours in c show Model 4 (see text), and represent how many MPa less the magnitude of σ_{11} is than compressive strength (CS).

A parametric study was performed to see what effect changes in P, σ_{11} and σ_{22} had on the magnitude of the maximum principal stresses and the orientation of resulting features around a hole in a plate (note that σ_{11} and σ_{22} represent deviatoric stresses). The distance of a feature from the center of the hole is given in magma source radii; the term "magma source" refers to the hole in the plate and could represent either a shallow magma chamber or the upper portion of

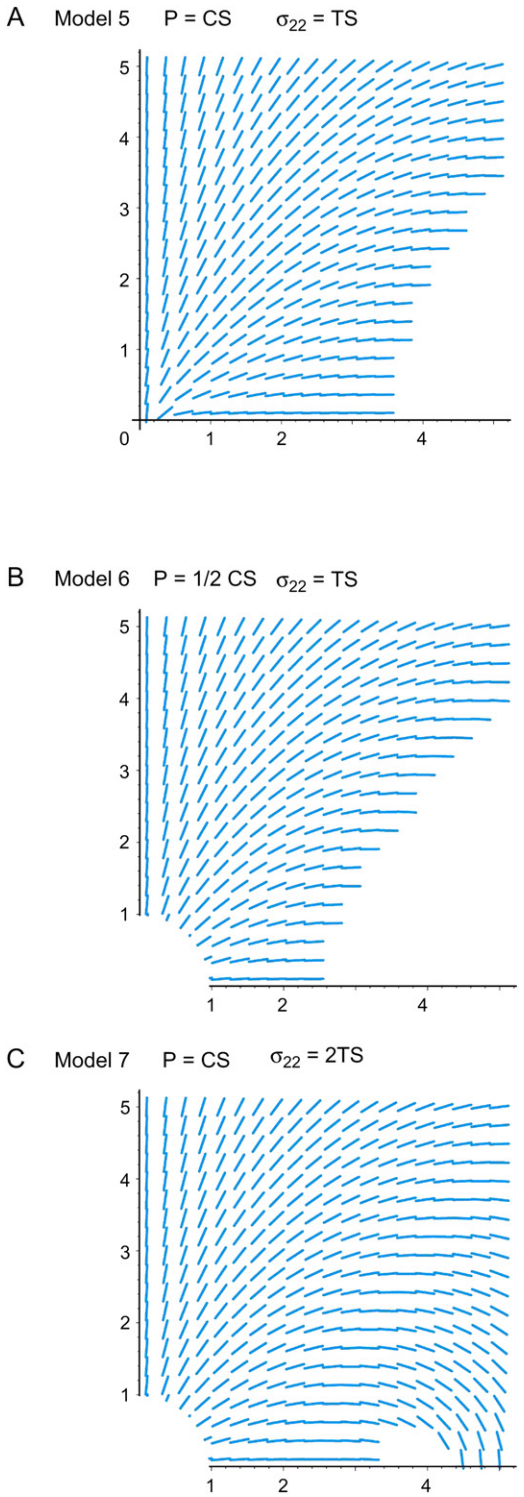

Fig. 9. Orientation and extent of structures in the presence of a uniaxial E-W tensile stress field. Blue are graben; there are no ridges. Axes are distance from the center of the magma source in units of magma source radius. Parameters vary as noted.

a magma conduit from a deeper reservoir. Sixteen models were run, in which the model input and setup can be arranged into four groups: 1) uniaxial compressive stress; 2) uniaxial tensile stress; 3) biaxial stress; and 4) a multiple hole system.

4.1. Model input: uniaxial compressive stress

The existence of the wrinkle ridges implies that at some point the regional compression exceeded the compressive strength of the material, so for this study it was assumed that σ_{11} is equal to compressive strength (CS), except where noted otherwise. In almost all of the models described below magma pressure P was equal to or less than CS; in all cases, when P was much greater than CS only radial graben could form. The maximum possible compressive strength for Venus rocks as determined by Schultz (1993) is 50 MPa. This is comparable to the magma pressure for shallow depths as determined by Koenig and Pollard (1998).

In the first model, magma pressure P and the N-S compression σ_{11} are equal (Fig. 8a). This model allows both ridges and graben to form radial to the volcano. Regardless of the magnitude of magma pressure and regional compression, graben form radially north and northeast, but the distance these graben extend from the volcano is dependent upon magma pressure magnitude (greater P yields longer graben). Ridges form radial to the volcano from N55E to N80E, regardless of the magnitude of the stresses. These stress parameters also indicate that north-south trending ridges should form from N40E to N55E, eventually curving toward the west from N30E to N40E.

In the second model magma pressure magnitude is twice the N-S compression (Fig. 8b). Graben formation occurs south to N60E, but graben extent is limited to within three magma source radii of the center of the hole. No radial ridges form.

In the third model the N-S compression is twice the magma pressure (Fig. 8c). Graben lengths to the north are reduced significantly, although they still extend some distance to the northeast. These stress parameters enable radial ridges to form from N55E to due east.

The fourth model is an adaptation of model 3, where the N-S compression is twice magma pressure but less than the compressive strength (Fig. 8c contours). Unlike situations where regional compression equals compressive strength, the ridge extent is limited. Radial ridges are still found from N55E to due east, but the distances they extend from the magma source are curtailed with increasing compressive strength. When the σ_{11} is more than 5 MPa less than the compressive strength, no ridges will form. With these stress parameters, the regional set of wrinkle ridges has stopped forming before radial ridge formation occurs.

4.2. Model input: uniaxial tensile stress

Extending roughly north-south through Irnini Mons is the rift system Badb Linea (Fig. 1). There are indications that this rift was active both before and after flows from the volcano. Although the rift was due to local extension, for areas close to Irnini the rift extension can be modeled as due to an east-west, tensile σ_{22}. The perturbation of a uniaxial, east-west tensile stress σ_{22} around a pressurized hole yields radial graben 360° around the hole when σ_{22} is equal to (model 5, Fig. 9a) or less than (model 6, Fig. 9b) the tensile strength (TS), although graben length is curtailed to the east and

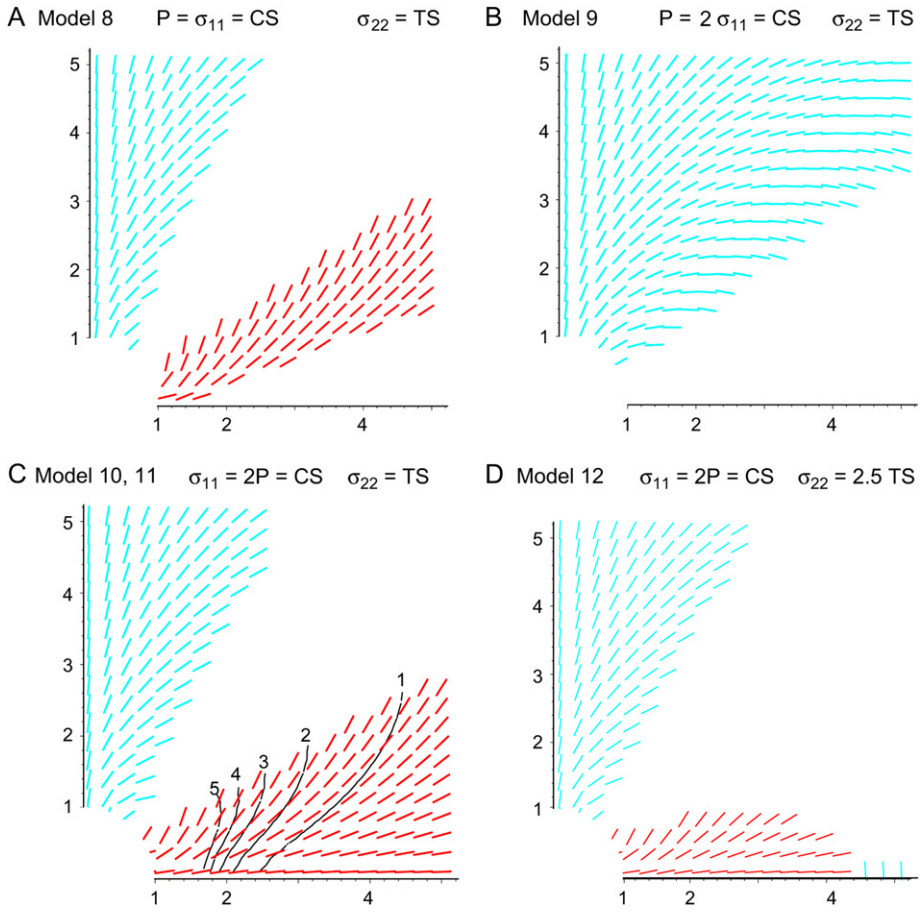

Fig. 10. Orientation and extent of structures in the presence of a biaxial stress field. Blue are graben, red are ridges. Axes are distance from the center of the magma source in units of magma source radius. Parameters vary as noted. Contours in c show model 11 (see text) and represent how many MPa less the magnitude of σ_{11} is than compressive strength (CS).

west. When σ_{22} is high (>twice the tensile strength), the radial graben loop back around on the hole, becoming circumferential east-west of the magma source, starting several magma source radii away (model 7, Fig. 9c).

There are no compressive circumferential stresses to form radial ridges in any of these three models. While a radial compressive stress is produced, it does not exceed the compressive strength of the material and no circumferential ridges form.

4.3. Model input: biaxial stress

In the eighth model a tensile E-W σ_{22} is added to a compressive N-S σ_{11}; magma pressure and σ_{11} are equal to the compressive strength (CS), while σ_{22} is equal to the tensile strength (TS). Both radial ridges and radial graben can form (Fig. 10a), similar to those produced by a uniaxial compressive N-S σ_{11} but without the eventual curving to the north and north-west (Fig. 8a–c). Radial ridges form from N55E to N80E; radial graben form from due north to N30E.

The ninth model has magma pressure magnitude equal to the compressive strength of the material, but twice the regional compression (Fig. 10b). Just as when P was twice σ_{11} in the unaxial case (Fig. 8b) only radial graben form, but the addition of a tensile σ_{22} equal in magnitude to the tensile material strength (TS) increases graben extent.

In the tenth model σ_{22} is still equal in magnitude to the tensile material strength, but the regional compression is equal to the compressive strength and twice the magma pressure (Fig. 10c). Radial ridges form from N60E to due east, while radial graben form from due north to N40E.

The eleventh model is an adaptation of model 10. The N-S compression is twice magma pressure but less than the compressive strength and σ_{22} is equal in magnitude to the tensile strength (Fig. 10c contours). The results are similar to those of the tenth model, but the distance the radial ridges extend is curtailed. The length the ridges reach depends on how much greater σ_{11} is than the compressive strength. When the difference is more than 5 MPa no radial ridges form.

The twelfth model has σ_{11} equal to the compressive material strength and twice the magma pressure; the tensile σ_{22} is twice the tensile strength (Fig. 10d). This model predicts short circumferential graben due east of the magma source, starting several magma source radii away from its center. Unlike in the uniaxial E-W tensile σ_{22} model (Fig. 9c), these circumferential graben are limited in length and are not connected to the radial graben.

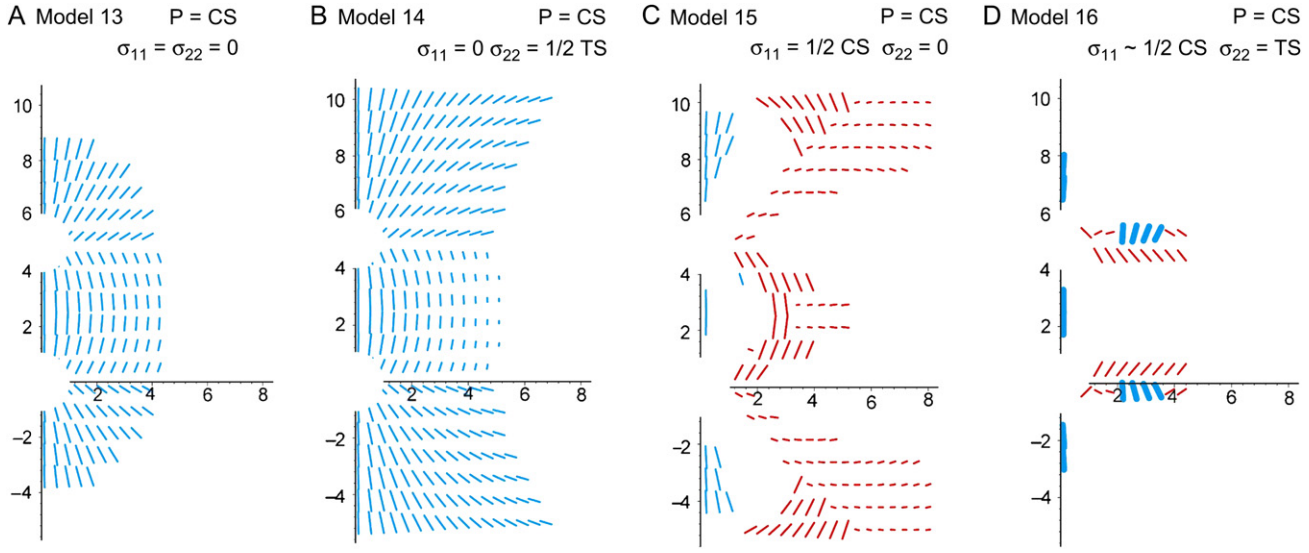

Fig. 11. Orientation and extent of structures that form around two holes aligned due north-south of each other in the presence of various regional stress fields. Blue are graben, red are ridges. Axes are distance from the center of the magma source in units of magma source radius. Parameters vary as noted.

4.4. Model setup: multiple pressurized holes

Anala Mons is a volcano to the south of Irnini Mons, aligned roughly parallel to the direction of regional compression. It can be modeled as a second pressurized hole. Anala flows truncate flows from Irnini (Fig. 1) and it has a more pristine form (Grimm and Phillips, 1992), indicating that it is the younger volcano. Badb Linea cuts through Anala flows as well as Irnini flows.

The interaction of two pressurized magma sources, without the presence of a significant regional stress field, yields radial graben to the north of the northern hole and to the south of the southern hole (model 13, Fig. 11a). In between the two holes are graben that are not radial to either hole, but rather connect them. These results are consistent with previous models that have explored the perturbation of regional stress fields around multiple, interacting holes (McKenzie et al., 1992).

The interaction of the two holes intensifies regional stresses. In those models where either uniaxial or biaxial stresses were applied to two north-south aligned holes (Fig. 11b–d), stresses equal to half material strength produce failure. Where there was no regional compression no ridges formed (model 14, Fig. 11b). But when there was a regional compression radial ridges formed, both when there was no tensile σ_{22} (model 15, Fig. 11c) and when there was (model 16, Fig. 11d).

5. Discussion

5.1. Model results

The parametric study shows that it is possible that compressional ridges can form radial to a pressurized hole in a homogeneous plate in the presence of a differential regional stress field. Nine of the sixteen models presented here result in radial ridges in the orientation observed around Irnini Mons. Single-hole models require a regional N-S compression that is equal to or greater than the magma pressure to allow the formation of radial ridges (models 1, 3, 4, 8, 10, 11 and 12). However, models 4 and 11 show that this σ_{11} can be as much as 5 MPa less than the compressive strength of the material. The two double-hole models that result in radial ridges (models 15 and 16) also have a regional N-S compression, but σ_{11} must have half the magnitude of the magma pressure or no graben can form, only ridges.

In both models four (Fig. 8c) and eleven (Fig. 10c) the magnitude of the regional compressive stress could be slightly less than the compressive strength of the material. If the regional compression is less than the material's compressive strength, wrinkle ridges will not form. However, the perturbation of the regional compression around a magma source would enhance the magnitude of the resulting circumferential compressive stress. In other words, radial ridges could form even after regional wrinkle ridge formation has ceased.

The twelfth model (Fig. 10d) can explain the presence of short circumferential graben parallel to Badb Linea. There are circumferential graben less than 50 km long and 1 km wide around Irnini Mons which first appear more than 130 km to the east of the summit graben. This short set of graben fits a model in which Badb Linea rifting and Irnini magma pressure were occurring concurrent with a north-south regional compression. These graben could form either coincident with wrinkle ridge formation (σ_{11} = compressive strength) or just after wrinkle ridge formation ceased ($\sigma_{11} = 1-5$ MPa < compressive strength). However, these features only form when the tensile σ_{22} is at least two and a half times the tensile strength of the material. Also, the extent of radial ridge formation is limited relative to the range of ridges in Figs. 8c and 10c.

A possible sequence of stress states that would result in features that match the geology to the northeast of Irnini Mons is:

1) $\sigma_{11} \geq$ P, $\sigma_{11} \leq$ CS, $\sigma_{22} = 0$: Radial ridge formation started prior to Badb Linea rifting (Fig. 8c), but possibly just after wrinkle ridge formation ceased.

2) $\sigma_{11} = 2P$, $\sigma_{11} \leq CS$, $\sigma_{22} = TS$: The start of Badb Linea rifting increases the extent to which radial graben form, but still allows the formation of radial ridges (Fig. 10c).

3) $\sigma_{11} \geq 2P$, $\sigma_{11} \leq CS$, $\sigma_{22} = 2.5$ TS: A peak in Badb Linea rifting restricts the extent of new radial ridges, while forming short circumferential graben (Fig. 10d).

4) $\sigma_{11} \ll CS$, $\sigma_{22} = < 1/2$ TS: None of the structure patterns created in the two-hole model match the observed features around Irnini Mons (Fig. 11), implying that the compressive stress responsible for the formation of regional wrinkle ridges had decreased significantly in magnitude (less than half the compressive strength) or ceased by the time the Anala magma chamber was active. The Badb Linea rifting must also have decreased significantly in magnitude by this time, or younger graben would have cut the radial ridges. However, it is likely that the perturbation of the reduced regional stresses around the double-hole system erased any radial ridges that may have formed to the south of Irnini Mons.

5.2. Tectonic inversion

A second possible scenario for radial ridge formation invokes the tectonically inverted graben theory of DeShon et al. (2000). In this scenario only radial graben formed around Irnini Mons. Later Irnini flows filled some of the graben and solidified. Magma pressure ceased and compression commenced, causing the solidified fill in those graben oblique to the compression direction to invert and form radial ridges.

While this scenario can account for ridges radial to Irnini Mons that are younger than the Irnini flows, it requires clarification. Regional north-south compression presumably created the regional set of east-west trending wrinkle ridges; this compression is at the right orientation to invert graben from N45E to N75E. However, there are no wrinkle ridges on the Irnini flows, which precludes their emplacement before wrinkle ridge formation unless the flow material is considerably stronger than the background regional plains. Thus, this scenario is only possible if wrinkle ridge formation took place well after the formation of Irnini Mons. Alternatively, inverted radial ridges could have formed during a second, smaller compressional event after wrinkle ridge formation had ended, but only if tectonic inversion does not require the same magnitude of compression that is required for material failure (Schultz, 1993).

5.3. Quadrant symmetry

While in the simple hole-in-a-plate model resultant stresses and any corresponding structures would be symmetric around the hole, at Irnini Mons the radial ridges are found only to the north-east of the volcano from N45E to N75E. This lack of symmetry may be due to the presence of structural complexities to the south and west of Irnini Mons (Fig. 1b). For example, the formation of Anala Mons directly south of Irnini would surely have erased any graben or ridges that would have formed around the older volcano. To the west of Irnini, Nehalennia Corona could have either inhibited radial ridge formation or covered radial ridges with associated flows. Anala and Nehalennia are representative of the complexities that need to be incorporated into the model to fully understand the sequence of events that resulted in the structures observed around Irnini Mons today.

6. Conclusion

In conclusion, the results of the first order model suggest that the existence of radial ridges on the Irnini flows can be mathematically accounted for as primary features that result from the warping of a regional stress field around a hole in a plate. The model implies that the regional north-south compression that caused the east-west trending wrinkle ridges was still active during the formation of Irnini Mons. A rough timeline for events in the region could be: 1) formation of east-west wrinkle ridges on regional plains; 2) coeval formation of graben radial to Irnini due to magma pressure and formation of radial ridges due to a combination of magma pressure and ongoing regional compression; 3) start of Badb Linea rifting and possible lessening of regional compression encourages graben formation at a broader range of azimuths; 4) cessation of magma pressure and formation of concentric graben at summit (Grimm and Phillips, 1992); and 5) formation of concentric wrinkle ridges, perhaps due to gravitational relaxation of the topographic rise (Grimm and Phillips, 1992; Basilevsky, 1994; Bilotti and Suppe, 1999). Comparison of the corresponding sequence of stress orientations to existing tectonic models for Venusian plains formation could help differentiate between opposing hypotheses. However, further modeling needs to be done, incorporating such concepts as material heterogeneity, an ellipsoidal magma source, lithospheric loading (McGovern and Solomon, 1998) and domical uplift and deflation, before any definitive statements on the formation of these unusual radial ridges can be made or before any timing issues can truly be resolved.

Acknowledgements

The author would like to thank Eric Grosfils for a thorough and useful review and an anonymous reviewer for comments and suggestions. The author would also like to thank George McGill and Michele Cooke for helpful discussions, technical aid, and support. Research reported in this paper was supported by NASA Planetary Geology and Geophysics Program grant NAG5-11649 to the University of Massachusetts, G.E. McGill PI.

References

Arvidson, R.E., Greeley, R., Malin, M.C., Saunders, R.S., Izenberg, N., Plaut, J.J., Stofan, E.R., Shepard, M.K., 1992. Surface modification of Venus as inferred from Magellan observations of plains. J. Geophys. Res. 97, 13303–13317.

Banerdt, W.B., 1986. Support of long wavelength loads on Venus and implications for internal structure. J. Geophys. Res. 91, 403–419.

Basilevsky, A.T., 1994. Concentric wrinkle ridge pattern around Sif and Gula (abstract). Lunar Planet. Sci. Conf. XXV, 63–64.

Basilevsky, A.T., Head, J.W., 1998. The geologic history of Venus: a stratigraphic view. J. Geophys. Res. 103, 8531–8544.

Basilevsky, A.T., Head, J.W., 2000. Geologic units on Venus: evidence for their global correlation. Planet Space Sci. 48, 75–111.

Basilevsky, A.T., Head, J.W., Schaber, G.G., Strom, R.G., 1997. The resurfacing history of Venus. In: Bougher, S.W., Hunten, D.M., Phillips, R.J. (Eds.), Venus II. Univ. Arizona Press, pp. 1047–1086.

Basilevsky, A.T., Head III, J.W., Ivanov, M.A., Kryuchkov, V.P., 1999. Impact craters on geologic units of northern Venus: implications for the duration of the transition from tessera to regional plains. Geophys. Res. Letts. 26, 2593–2596.

Bilotti, F., Suppe, J., 1999. The global distribution of wrinkle ridges on Venus. Icarus 139, 137–157.

Campbell, B.A., 1999. Surface formation rates and impact crater densities on Venus. J. Geophys. Res. 104, 21951–21955.

Campbell, B.A., 2002. Radar Remote Sensing of Planetary Surfaces. Cambridge University Press, Cambridge, UK, 331 pp.

Collins, G.C., Head, J.W., Basilevsky, A.T., Ivanov, M.A., 1999. Evidence for rapid regional plains emplacement on Venus from the population of volcanically embayed craters. J. Geophys. Res. 104, 24121–24140.

Cyr, K.E., Melosh, H.J., 1993. Tectonic patterns and regional stresses near Venusian coronae. Icarus 102, 175–184.

DeShon, H.R., Young, D.A., Hansen, V.L., 2000. Geologic evolution of southern Rusalka Planitia, Venus. J. Geophys. Res. 105, 6983–6995.

Ernst, R.E., Head, J.W., Parfitt, E., Grosfils, E.B., Wilson, L., 1995. Giant radiating dyke swarms on Earth and Venus. Earth Sci. Rev. 39, 1–58.

Ernst, R.E., Grosfils, E.B., Mege, D., 2001. Giant dike swarms: Earth, Venus and Mars. Ann. Rev. Earth Planet. Sci. 29, 489–534.

Ernst, R.E., Desnoyers, D.W., Head, J.W., Grosfils, E.B., 2003. Graben-fissure systems in Guinevere Planitia and Beta Regio (264–312°E, 24–60°N), Venus and implications for regional stratigraphy and mantle plumes. Icarus 164, 282–316.

Grimm, R.E., Phillips, R.J., 1992. Anatomy of a venusian hot spot: geology, gravity and mantle dynamics of Eistla Regio. J. Geophys. Res. 97, 16035–16054.

Grindrod, P.M., Nimmo, F., Stofan, E.R., Guest, J.E., 2005. Strain at radially fractured centers on Venus. J. Geophys. Res. 110, doi:10.1029/2005JE002416.

Grosfils, E.B., Head, J.W., 1994. The global distribution of giant radiating dike swarms on Venus: implications for the global stress state. Geophys. Res. Lett. 21, 701–704.

Grosfils, E.B., Head, J.W., 1997. Magma Reservoir Failure: Implications for Volcano Growth on Venus and Mars. LPSC XXVIII, abs. 1163 (CD-ROM). Lunar Planet. Inst., Houston, TX.

Gudmundsson, A., 1984. Formation of dykes, feeder-dykes, and the intrusion of dykes from magma chambers. Bull. Volcanol. 47, 537–550.

Gudmundsson, A., 1986. Possible effect of aspect ratios of magma chambers on eruption frequency. Geology 14, 991–994.

Gudmundsson, A., 1988. Effect of tensile stress concentration around magma chambers on intrusion and extrusion frequencies. Jour. Volcanol. Geotherm. Res. 35, 179–194.

Guest, J.E., Stofan, E.R., 1999. A new view of the stratigraphic history of Venus. Icarus 139, 55–66.

Hansen, V.L., Willis, J.J., Banerdt, W.B., 1997. Tectonic overview and synthesis. In: Bougher, S.W., Hunten, D.M., Phillips, R.J. (Eds.), Venus II. Univ. Arizona Press, pp. 797–844.

Hauck II, S.A., Phillips, R.J., Price, M.H., 1998. Venus: crater distribution and plains resurfacing models. J. Geophys. Res. 103, 13635–13642.

Head, J.W., Wilson, L., 1992. Magma reservoirs and neutral buoyancy zones on Venus: implications for the formation and evolution of volcanic landforms. J. Geophys. Res. 97, 3877–3903.

Head, J.W., Crumpler, L.S., Aubele, J.C., Guest, J.E., Saunders, R.S., 1992. Venus volcanism: classification of volcanic features and structures, associations and global distribution form Magellan data. J. Geophys. Res. 97, 13153–13197.

Jaeger, J.C., Cook, N.G.W., 1979. Fundamentals of Rock Mechanics. Chapman Hall, New York, 593 pp.

Koenig, E., Pollard, D.D., 1998. Mapping and modeling of radial fracture patterns on Venus. J. Geophys. Res. 103, 15183–15202.

McGill, G.E., 1993. Wrinkle ridges, stress domains, and kinematics of Venusian plains. Geophys. Res. Lett. 20, 2407–2410.

McGill, G.E., 2000. Geologic map of the Sappho Patera (V20) quadrangle, Venus, U.S. Geol. Survey, Geol. Investigations Map I-2627.

McGovern, P.J., Solomon, S.C., 1998. Growth of large volcanoes on Venus: mechanical models and implications for structural evolution. J. Geophys. Res. 103 (E5), 11,071–11,101.

McKenzie, D., McKenzie, J.M., Saunders, R.S., 1992. Dike emplacement on Venus and Earth. J. Geophys. Res. 97, 15977–15990.

McKinnon, W.B., Zahnle, K.J., Ivanov, B.A., Melosh, H.J., 1997. Cratering on Venus: models and observations. In: Bougher, S.W., Hunten, D.M., Phillips, R.J. (Eds.), Venus II. Univ. Arizona Press, pp. 969–1014.

Muller, O.H., Pollard, D.D., 1977. The state of stress near Spanish Peaks, Colorado, determined from a dike pattern. Pure Appl. Geophys. 115, 69–86.

Ode, H., 1957. Mechanical analysis of the dike pattern of the Spanish Peaks Area, Colorado. GSA Bull. 68, 567–576.

Parfitt, E.A., Head, J.W., 1993. Buffered and unbuffered dike emplacement on Earth and Venus: implications for magma reservoir size, depth and rate of magma replenishment. Earth Moon Planets 61, 249–281.

Phillips, R.J., Hansen, V.L., 1994. Tectonic and magmatic evolution of Venus. Ann. Rev. Earth Planet Sci. 22, 597–656.

Phillips, R.J., Arvidson, R.E., Boyce, J.M., Campbell, D.B., Guest, J.E., Schaber, G.G., Soderblom, L.A., 1991. Impact craters on Venus: initial analysis from Magellan. Science 252, 288–297.

Phillips, R.J., Raubertas, R.F., Arvidson, R.E., Sarkar, I.C., Herrick, R.R., Izenberg, N., Grimm, R.E., 1992. Impact craters and Venus resurfacing history. J. Geophys. Res. 97, 15923–15948.

Pollard, D.D., Holzhausen, G., 1979. On the mechanical interaction between a fluid-filled fracture and the Earth's surface. Tectonophysics 53, 27–57.

Price, M.H., 1997. Free at last: a perspective on the CSR constraint, Geodynamics of Venus: Evolution and Current State, Chapman Conf., Snowmass at Aspen, pp. 7–8.

Sandwell, D.T., Johnson, C.L., Bilotti, F., Suppe, J., 1997. Driving forces for limited tectonics on Venus. Icarus 129, 232–244.

Schaber, G.G., Strom, R.G., Moore, H.J., Soderblom, L.A., Kirk, R.L., Chadwick, D.J., Dawson, D.D., Gaddis, L.R., Boyce, J.M., Russell, J., 1992. Geology and distribution of impact craters on Venus: what are they telling us? J. Geophys. Res. 97, 13257–13301.

Schultz, R.A., 1993. Brittle strength of basaltic rock masses with applications to Venus. J. Geophys. Res. 98, 10883–10895.

Solomon, S.C., Bullock, M.A., Grinspoon, D.H., 1999. Climate change as regulator of tectonics on Venus. Science 286, 87–90.

Stofan, E.R., Sharpton, V.L., Schubert, G., Baer, G., Bindschadler, D.L., Janes, D.M., Squyres, S.W., 1992. Global distribution and characteristics of coronae and related features on Venus – implications for origin and relation to mantle processes. J. Geophys. Res. 97, 13347–13378.

Strom, R.G., Schaber, G.G., Dawson, D.D., 1994. The global resurfacing of Venus. J. Geophys. Res. 99, 10899–10926.

Sturkell, E., Einarsson, P., Sigmundsson, F., Hreinsdottir, S., Geirsson, H., 2003. Deformation of Grimsvotn volcano, Iceland: 1998 eruption and subsequent inflation. Geophys. Res. Lett. 30 (4), 1182, doi:10.1029/2002GL016460.

Turcotte, D.L., Roberts, D.C., Malamud, B.D., 1998. Cratering statistics on Venus. LPSC XXIX, abs. 1703 (CD-ROM). Lunar Planet. Inst., Houston, TX.

Zahnle, K., McKinnon, W., 1996. Age of the surface of Venus. Bull. Am. Astron. Soc. 28, 1119.